ChemComm

This is an *Accepted Manuscript*, which has been through the Royal Society of Chemistry peer review process and has been accepted for publication.

Accepted Manuscripts are published online shortly after acceptance, before technical editing, formatting and proof reading. Using this free service, authors can make their results available to the community, in citable form, before we publish the edited article. We will replace this *Accepted Manuscript* with the edited and formatted *Advance Article* as soon as it is available.

You can find more information about *Accepted Manuscripts* in the **Information for Authors**.

Please note that technical editing may introduce minor changes to the text and/or graphics, which may alter content. The journal's standard **Terms & Conditions** and the **Ethical guidelines** still apply. In no event shall the Royal Society of Chemistry be held responsible for any errors or omissions in this *Accepted Manuscript* or any consequences arising from the use of any information it contains.

Journal Name

COMMUNICATION

Plasmon-Enhanced Fluorescence of PbS Quantum Dots for Remote Near-Infrared Imaging

Ke Wu[a], Junpei Zhang[b], Shanshan Fan[b], Juan Li[a], Chao Zhang[a], Keke Qiao[c], Lihua Qian[a],[*], Junbo Han[b], Jiang Tang[c], Shuai Wang[d],[*]

Gold nanoparticles with nanoscale protrusions can be synthesized by seed-mediated growth in favor of tuning surface plasmon band towards near-infrared regime. Electromagnetic field enhancement makes significant contribution to improve fluorescence emission of PbS quantum dots in the near-infrared window, identifying its application for remote imaging by collecting the scattered fluorescence of their hybrids.

Excitation of surface plasmon resonance (SPR) can generate huge electromagnetic field on the surfaces of metal nanoparticles (NPs),[1,2] which holds many promising applications including plasmon-enhanced fluorescence (PEF),[3-5] plasmon-enhanced Raman scattering (PERS),[6,7] biological imaging,[8-10] and thermo-physical therapy of the tumor[11] etc. Fluorescence emission intrinsically depends on the absorption and emitting cross-section of the fluorophores detected, such as organic molecules[12,13] and quantum dots (QDs).[14-17] Meanwhile, fluorescence intensity is extrinsically a function of electromagnetic field where the fluorophores situate. When the fluorophores are resided in close proximity to metal surface, fluorescence emission behaves differently from it would in free space. In the optimal experimental configurations, more photons can be trapped by the fluorophores, resulting in more electrons that can be excited towards high energy levels. On the other hand, increased radiative relaxation of the excited fluorophores occurs as energy is coupled into surface plasmons on the metal surface.[2,18]

To enhance the fluorescence emission of the fluorophores, the optimal location of SPR band becomes the first consideration. So far, gold nanostructures with distinct morphologies, such as metallic grating,[19] nanorods[20,21] and nanopores[22] etc, have reported to enhance the fluorescence emission of some organic molecules.

a School of Physics, Huazhong University of Science and Technology, Wuhan, 430074, China
b Wuhan National High Magnetic Field Center, Huazhong University of Science and Technology, Wuhan, 430074, China
c Wuhan National Laboratory for Optoelectronics (WNLO), Huazhong University of Science and Technology, Wuhan,430074, China
d School of Chemistry and Chemical Engineering, Huazhong University of Science and Technology, Wuhan, 430074, China
Electronic Supplementary Information (ESI) available: Experimental procedures and supporting figures are listed. See DOI: 10.1039/c000000x/

While only few investigations focus on the enhanced fluorescence of QDs including CdTe,[23] CdSe,[24,25] and Si QDs,[26,27] especially the enhanced fluorescence of the QDs in near-infrared (NIR) regimes.[28] In comparison with the PEF in visible window, the enhanced fluorescence excited and emitted in the NIR regimes holds the potential applications in biological sensing,[29-31] cellular imaging[32] and remote tacking of the drug delivery or release[33] due to the transparency of human skin within this window. In our previous investigation, silver nanowire is applied as the optical antenna to enhance the fluorescence spectroscopy of CdTe QDs, while emitting behavior significantly depends on laser polarization because different plasmonic modes are excited within anisotropic nanowire. PbS QDs have the fluorescence emission under the excitation of the NIR laser, and they can serve as the fluorescence label for cell imaging. To improve the brightness of PbS QDs and imaging depth, isotropic metal NPs with the SPR band at NIR regime are required to enhance fluorescence emission of PbS QDs that is independent of laser polarization. Herein, we demonstrate the precise control over the nearly-isotropic geometries of Au NPs during the seed-mediated growth. The plasmon band of Au NPs can be tuned from visible to NIR regime, so that they can be utilized to enhance the fluorescence signal of PbS QDs with the excitation of the NIR laser. This optimized performance facilitates the direct imaging of the PbS QDs by remotely collecting their scattered fluorescence.

Gold seeds with a diameter of 5 nm are synthesized by chemical reduction in aqueous solution cooled by the ice.[34] Gold NPs with the larger diameters are fabricated by controlling the secondary growth of Au seeds.[35] Figure 1 represents the typical morphology of Au NPs with an average diameter of ~170 nm according to the statistical analysis. All the NPs with many nanoscale protrusions exhibit the shape of urchin as shown in Fig. 1(a). Most protrusions have the sharp apex, whose curvature can be as small as ~5 nm. Selected area electron diffraction of an individual NP represents the discontinuous diffraction ring, implying that Au NP consists of many polycrystals rather than single crystal. These polycrystals usually result from the secondary growth onto the primary Au seeds.[36] Geometrical parameters including nanoparticle size and surface roughness normally depend on the concentrations of Au seeds and surface agents in aqueous solution during the secondary growth. In this work, by adjusting the concentration of Au seeds in the growth solution, a monotonic tailoring of nanoparticle size from 170 to 50

nm can be achieved as shown in Fig. 1(b), 1(c) and 1(d). Interestingly, the nanoscale protrusions within each type of Au NP are still remaining although Au NP is as small as 50 nm.
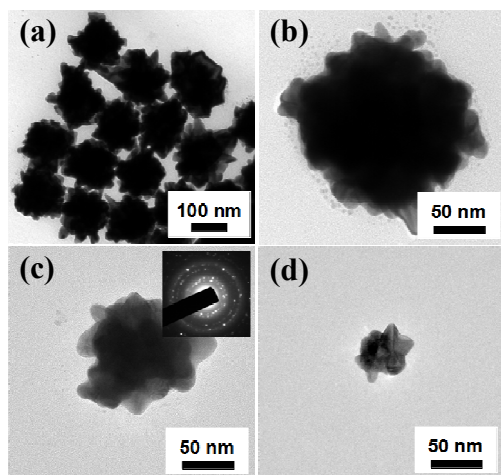
Fig. 1 TEM images of Au NPs with different surface morphologies. (a) Typical microstructure of Au NPs with a shape of urchin. (b-d) Gold NPs with various diameters. The inset in Fig. 1(c) is the selected area electron diffraction of an individual Au NP.

Figure 2(a) illustrates exinction spectra of Au NPs with various diameters, each of which exhibits an individual extinction peak, implying the uniform size distribution. This exinction peak results from the excitation of SPR. The SPR band monotonically shifts from 606 to 826 nm with the decreasing seed volume from 280 to 40 ml. The linear relationship between the position of SPR band and seed volume as shown in Fig. 2 (b) can offer a reliable experimental procedure to tune the location of SPR band towards the NIR window. This well-tuned feature of SPR band provides us an opportunity to enhance the fluorescence emission of PbS QDs in the NIR region.

For PbS QDs located nearby metal nanostructures, their enlarged distance will make a continuous transition from fluorescence quenching to fluorescence enhancement. In this work, silica (SiO_2) is deposited onto the surface of Au NPs as a spacer to isolate PbS QDs. Figure 3 shows that Au NPs can be covered by SiO_2 shell, whose thickness almost keeps a constant independent on the local morphology and curvature of Au NPs. The detailed characterizations indicate that SiO_2 is in amorphous state as shown in Fig. 3(e). Therefore, the thickness of SiO_2 shell can be precisely tuned from 5 to 20 nm by using different doses of tetraethylorthosilicate (TEOS), so that fluorescence intensity of PbS QDs can be optimized by tuning the thickness of SiO_2 spacer. Most PbS QDs have the average size of ~4.7 nm according to statistical analysis as shown in Fig. S1. In order to observe the distribution of PbS QDs onto Au@SiO_2 NPs for TEM observations, a drop of the aqueous hybrid is dispersed onto carbon supported copper grid until the completion of water evaporation. The PbS QDs attached onto Au@SiO_2 NPs as shown in Fig. 3(f) have the comparable size (it is evidenced by the lattice fringes in the inset) with free PbS QDs in Fig. S1. This indicates that the aggregation of PbS QDs toward the larger size cluster in the aqueous mixture or on the supported grid does not occur.

For avoiding the possible aggregation of PbS QDs and enhancing the spectrum comparability to great extent, all the fluorescence spectra are collected in aqueous solution, so that the PbS QDs can be considered to swim around the Au@SiO_2 NPs. When the hybrid consisting of PbS QDs and bare Au NPs without SiO_2 spacer, fluorescence intensity is slightly weaker than that of pure QDs,

indicating the fluorescence quenching occurs. When one increases the thickness of SiO_2 shell from 0 to 10 nm, fluorescence intensity increases by a magnitude of 5~6 times as shown in Fig. 4(a). Maximum fluorescence emission can be obtained when the thickness of SiO_2 shell is 10 nm, and the subsequent decrement of fluorescence intensity is observed with further thickening (Fig. 4(b)). It must be noted that the concentrations of Au NPs or Au@SiO_2 NPs and PbS QDs in each aqueous solution in Fig. 4(a) are $\sim 1.8 \times 10^{10}$ / ml and $\sim 4 \times 10^{14}$ / ml respectively, which can assure the reliable comparison of fluorescence intensity.
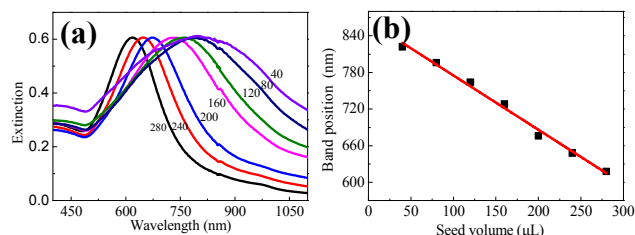
Fig. 2 (a) Extinction spectra of Au NPs with distinct diameters. (b) The variation of the SPR band position of Au NPs with the seed volume involved during seed-mediated growth, and a linear relationship can be fitted.
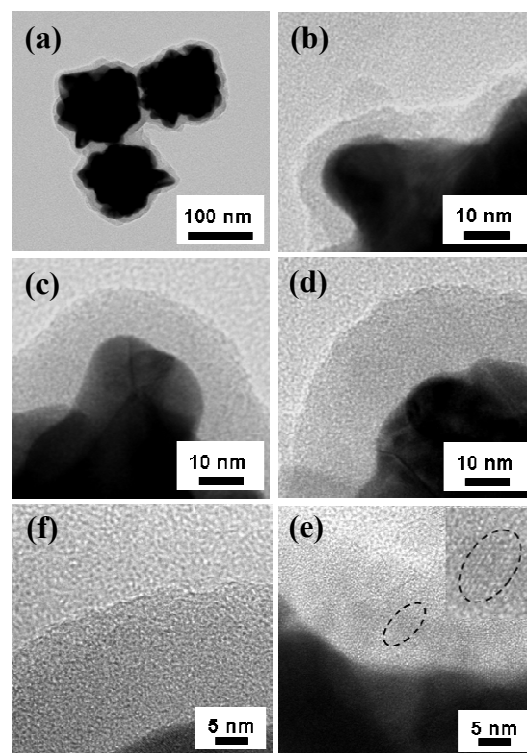
Fig. 3 TEM images of Au@SiO_2 NPs with tunable shell thicknesses. (a) Au NP uniformly coated by SiO_2. (b-d) The thicknesses of SiO_2 coated onto the Au NPs are 5, 10 and 20 nm, respectively. (e) High resolution TEM image of pure SiO_2 coated onto Au NPs. (f) High resolution TEM image of PbS QDs hybridized onto Au@SiO_2 NP. The circled regions are PbS QDs. The inset Fig. 3(f) is the magnified image of PbS QDs.

In order to clarify the intrinsic mechanism on fluorescence enhancement, fluorescence spectroscopy can be collected at the same experimental configuration except for selecting Au NPs with different SPR bands. During spectra collection, the laser with the

same wavelength is utilized. Fluorescence intensity as shown in Fig. 4(c) exhibits the significant reduction when SPR band of Au NPs is changed from 826 to 606 nm, implying that fluorescence enhancement is really related to the electromagnetic fields due to SPR excitation of Au NPs. (The PbS QDs concentration within the aqueous solution is identical for each spectrum acquisition, ensuring the total quantity of PbS QDs in the optical path is a constant. Optical path diagram is shown in Fig. S2)

Fluorescence emission of PbS QDs near the Au NPs mainly depends on two factors: field enhancement and an increment in the intrinsic decay rate of fluorophores. The first factor promotes excitation rates, but does not modify the fluorescence lifetime of the PbS QDs. Fluorescence intensity is usually proportional to the square of local electromagnetic fields where the QDs reside. In order to quantitatively evaluate field enhancement, finite difference time domain (FDTD) simulations conduce to calculate the extinction spectrum of an individual Au NP and estimate its field distributions in the surrounding medium.[37] Field distribution nearby the apex of an individual Au NP exhibits 5~6 times enhancement as shown in Fig. S3 (the exact value depends on the curvature of sharp apex). By considering the exponential attenuation of electromagnetic fields normal to metal surface, field enhancement at a distance of 10 nm away from the surface of Au NPs exhibits 2~4 times difference. In theory, two powers of field enhancements correspond to 4~16 times in fluorescence intensity, which is comparable with the experimental data. The second factor changes the quantum yield and lifetime of the fluorophore. Fluorescence lifetime of QDs hybridized onto Au NPs is implemented using time-correlated single photon counting by plotting a histogram of time lags between the excitation pulses and the detected fluorescence photons. Experimental results in Fig. 4(d) indicate the radiation decay rate modification of the PbS QDs in close proximity to the Au NPs.

For pure PbS QDs, single-exponential function can be utilized to fit their lifetime of PbS QDs in Fig. S4 ($\tau_1 = 4.51$ ns). While for the aqueous solution consisting of Au@SiO$_2$ NPs and PbS QDs, an additional decay mechanism might exist due to the SPR excitation. Therefore, we can use double-exponential function to fit their lifetime. Herein, τ_1 is fixed as 4.51 ns, while τ_2 is flexible to describe the fluorescence emission of PbS QDs affected by the near-field coupling between SPR of Au@SiO$_2$ NPs.[38] Therefore, τ_2 results from the PbS QDs located in the local field of Au NPs. We observed a considerably small lifetime τ_2 of 0.45 ns when PbS QDs are mixed with Au NPs without the SiO$_2$ spacer. In this case, the fluorescence decay is faster than free PbS QDs, implying energy transfer at the interface between Au NPs and PbS QDs and local field enhancement on the surface of Au NPs. Energy transfer becomes weaker and field enhancement becomes relatively dominant when SiO$_2$ spacer becomes thicker towards 10 nm, so that τ_2 of 0.30 ns can be observed. The significant reduction of lifetime implies that the enhanced recombination rate of PbS QDs because of their coupling with SPR of Au NPs, which is also detected in CdSe QDs.[39]

To prove the advantage of urchin-like Au NPs in comparison with Au NPs with smooth surfaces, fluorescence spectra are also collected from Au NPs with different surface morphologies while the comparable diameter (~55 nm) and the same SiO$_2$ shell (10 nm) (see Fig. S5). It indicates that Au NPs with the rough surfaces have the larger fluorescence enhancement for PbS QDs than Au NPs with the smooth surfaces. Fluorescence intensity is comparable for each curve because both the quantity of PbS QDs within optical path and experimental parameter during spectrum acquisition are identical.

In our experiment, the PbS QDs can be considered to swim around the Au@SiO$_2$ NPs, and there exists an effective fluorescence enhancement distance between the PbS QDs and the Au@SiO$_2$ NPs under laser irradiation. Thus only PbS QDs within the local field of

the Au@SiO$_2$ NPs will make the effective contribution to the overall fluorescence enhancement, while free QDs far away from Au@SiO$_2$ NPs have negligible contributions to signal enhancement. This might be the reason that the fluorescence enhancement in this work is weaker than the experiment results reported in some previous investigations.[13-14] Meanwhile, experimental enhancement factor (~2) of Au@SiO$_2$ NPs is smaller than the maximum factor estimated by FDTD simulations (4~16). The optimized distance between Au@SiO$_2$ NPs and QDs usually depends on many factors: the aqueous or solid states of their hybrids, the exact diameter of Au NPs, and surface roughness of Au NPs. In our experiments, the aqueous solution consisting of Au@SiO$_2$ NPs and PbS QDs is utilized to characterize magnitude of fluorescence enhancement. In this case, most QDs might be not directly attached onto the surface of Au@SiO$_2$ NPs, which is different from the hybrid consisting of the Au@SiO$_2$ NPs and dye molecules that are linked by some functionalized molecules. In the latter case, the exact distance between NPs and QDs should be smaller than that in the aqueous solution. Therefore, the optimized thickness of SiO$_2$ shell is a little smaller than the NPs/dye distances where largest fluorescence enhancement is observed.[13]

In principle, fluorescence enhancement mainly results from both excitation and emission enhancement by Au NPs. In our investigations, Au NPs exhibit the sharp apex, therefore the near-field enhancement can result from a combination of lightning rod effect and plasmonic resonance[1,2]. At first, larger field enhancement nearby the sharper apex can be observed in the FDTD simulation
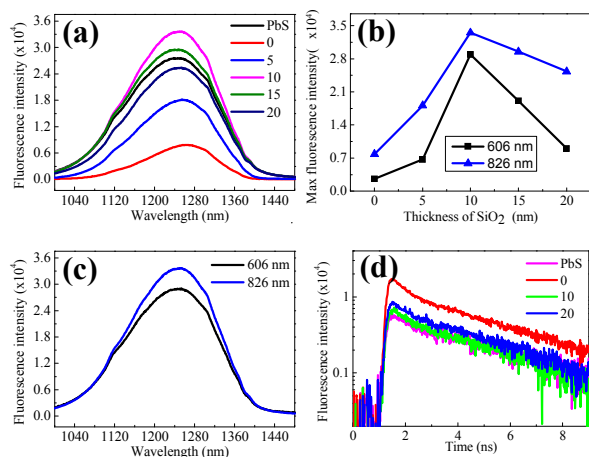
Fig. 4 (a) Fluorescence spectra of PbS QDs hybridized onto the surface of Au NPs (band position at 826 nm) with different thickness of SiO$_2$. (b) The variation of fluorescence intensity with the thickness of SiO$_2$ shells. (c) The fluorescence spectra of PbS QDs hybridized onto Au NPs with distinct SPR bands (band position: 606 and 826 nm) while the same shell thickness of 10 nm. (d) Temporal intensity decay of PbS QDs on different Au@SiO$_2$ NPs and pure PbS QDs.

(see Fig. S3). Secondly, on resonance of SPR will induce larger field enhancement than off resonance, which can be confirmed by collecting the fluorescence of PbS QDs hybridized onto Au@SiO$_2$ NPs with different SPR bands. The fluorescence intensity from 170 nm Au NPs is larger than that from 50 nm Au NPs, and this phenomenon results from larger NPs holding SPR band much closer to the wavelength of the exciting laser (826 nm) and the emission wavelength (1225 nm) as well (see Fig. S6). Thus, high enhancement that we observe here is most likely a combination of excitation and emission enhancements in the optimal shell thickness.

The other factor to affect fluorescence emission is the changing decay rate of fluorophore, which can be reflected by its lifetime[2,18]. In the hybrid consisting of Au NPs and PbS QDs, the lifetime τ_2 is significantly reduced in comparison with the τ_1 of pure PbS QDs. This is well related to the field enhancement due to SPR excitation and fluorescence quenching due to the energy transfer at Au/PbS interfaces. While for the hybrid consisting of Au-SiO$_2$ NPs with 10 nm thick shells and PbS QDs, fluorescence quenching will become weaker because energy transfer at Au/PbS interfaces is partially suppressed, and field enhancement resulted from SPR excitation will make more contribution to the effective path of radiating decay in comparison with non-radiating decay due to fluorescence quenching. In general, our present data implies that PEF observed in PbS QDs is primarily affected by the field enhancement on the surfaces of Au@SiO$_2$ NPs.
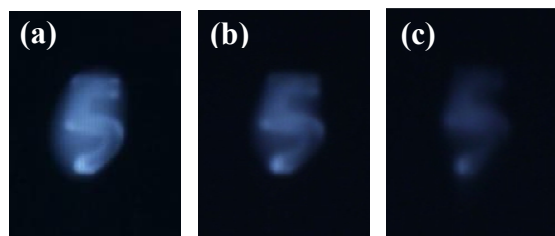
Fig. 5 The NIR imaging of a character of "5" written by Au@SiO$_2$-PbS QDs hybrid. The images are taken from different distances of 35, 50, 70 cm.

The results described above indicate that the fluorescence emission of PbS QDs can be enhanced when the thickness of SiO$_2$ spacer is optimized. This property offers us one opportunity to image the QDs/Au@SiO$_2$ NPs hybrid by collecting the scattered fluorescence remotely. Figure 5 represents the optical images of QDs/Au@SiO$_2$ NPs hybrid with a character of "5" (SiO$_2$ shell is 10 nm in thickness) taken from different distances in a range of 35~70 cm. This character can be clearly seen when the hybrid label is 35 cm away from the CCD. The remote imaging of PbS QDs at NIR region might bring some applications including the biological imaging, the real-time tracking of drug delivery. Especially human skin is transparent at the NIR region, which will benefit to the medical diagnosis, thermotherapy and in-vivo imaging of the tumor.

In summary, fluorescence imaging in NIR window has found widespread applications in biological science including clinical diagnosis and real-time tracking of internal medicine. Gold NPs with nanoscale protrusions/or surface roughness are fabricated by controlling the kinetics on the secondary growth of Au seeds. Surface plasmon band tuned from 606 to 826 nm represents the linear dependence onto the amount of Au seeds during chemical synthesis, with a subsequence of its monotonic shift towards NIR region by enlarging the NP diameter from 50 to 170 nm. Gold NPs with the plasmon band at 826 nm can enhance the fluorescence emission of PbS QDs excited by the NIR laser, so that remote imaging of QDs can be achieved by acquisition of the scattered fluorescence at a wavelength of 1225 nm.

Acknowledgements

Notes and references

1 W. Wang, Z. P. Li, B. H. Gu, Z. Y. Zhang, and H. X. Xu, *ACS Nano*, 2009, **3**, 3493.

2 A. Hartschuh, *Angew. Chem. Int. Edit.*, 2008, **47**, 8178.

3 F. Tam, G. P. Goodrich, B. R. Johnson, and N. J. Halas, *Nano Lett.*, 2007, **7**, 496.

4 X. Y. Lang, P. F. Guan, L. Zhang, T. Fujita, and M. W. Chen, *Appl. Phys. Lett.* 2010, **96**, 073701.

5 S. H. Guo, D. G. Britti, J. J. Heetderks, H. C. Kan, and R. J. Phaneuf, *Nano Lett.*, 2009, **9**, 2666.

6 M. Moskovits, *Rev. Mod. Phys.*, 1985, **57**, 783.

7 D. A. Weitz, S. Garoff, J. I. Gersten, and A. Nitzan, *J. Chem. Phys.*, 1983, **78**, 5324.

8 C. D. Geddes, H. Cao, I. Gryczynski, Z. Gryczynski, J. Y. Fang, and J. R. Lakowicz, *J. Phys. Chem. A*, 2003, **107**, 3443.

9 Y. F. Kong, J. Chen, F. Gao, R. Brydson, B. Johnson, G. Heath, Y. Zhang, L. Wu, and D. J. Zhou, *Nanoscale*, 2013, **5**, 1009.

10 Z. Li, Q. Sun, Y. Zhu, B. Tan, Z. P. Xu, and S. X. Dou, *J. Mater. Chem. B*, 2014, **2**, 2793.

11 H. Y. Chen, S. L. Li, B. W. Li, X. Y. Ren, S. N. Li, D. M. Mahounga, S. S. Cui, Y. Q. Gu, and S. Achilefu, *Nanoscale*, 2012, **4**, 6050.

12 Y. Fu, J. Zhang, K. Nowaczyk, and J. R. Lakowicz, *Chem. Commun.*, 2013, **49**, 10874.

13 P. Reineck, D. Gomez, S. H. Ng, M. Karg, T. Bell, P. Mulvaney, and U. Bach, *ACS Nano*, 2013, **7**, 6636.

14 L. Zhang, Y. K. Song, T. Fujita, Y. Zhang, M. W. Chen, and T. H. Wang, *Adv. Mater.*, 2014, **26**, 1289.

15 O. Kulakovich, N. Strekal, A. Yaroshevich, S. Maskevich, S. Gaponenko, I. Nabiev, U. Woggon, and M. Artemyev, *Nano Lett.*, 2002, **2**, 1449.

16 K. Ray, R. Badugu, and J. R. Lakowicz, *J. Am. Chem. Soc.*, 2006, **128**, 8998.

17 E. Hwang, I. I. Smolyaninov, and C. C. Davis, *Nano Lett.*, 2010, **10**, 813.

18 C. H. Wang, C. W. Chen, Y. T. Chen, C. M. Wei, Y. F. Chen, C. W. Lai, M. L. Ho, P. T. Chou, and M. Hofmann, *Appl. Phys. Lett.*, 2010, **96**, 071906.

19 K. Tawa, H. Hori, K. Kintaka, K. Kiyosue, Y. Tatsu, and J. Nishii, *Opt. Exp.*, 2008, **16**, 9781.

20 H. F. Yuan, S. Khatua, P. Zijlstra, M. Yorulmaz, and M. Orrit, *Angew. Chem. Int. Ed.*, 2013, **52**, 1217.

21 M. Fu, L. H. Qian, H. Long, K. Wang, P. X. Lu, Y. P. Rakovich, F. Hetsch, A. S. Susha, and A. L. Rogach, *Nanoscale*, 2014, **6**, 9192.

22 X. Y. Lang, L. H. Qian, P. F. Guan, J. Zi, and M. W. Chen, *Appl. Phys. Lett.*, 2011, **98**, 093701.

23 A. E. Ragab, A. S. Gadallah, T. Da Ros, M. B. Mohamed, and I. M. Azzouz, *Opt. Commun.*, 2014, **314**, 86 .

24 Y. H. Chan, J. X. Chen, S. E. Wark, S. L. Skiles, D. H. Son, and J. D. Battea, *ACS Nano*, 2009, **3**, 1735.

25 K. Munechika, Y. Chen, A. F. Tillack, A. P. Kulkarni, I. J. L. Plante, A. M. Munro, and D. S. Ginger, *Nano Lett.*, 2010, **10**, 2598.

26 N. A. Harun, M. J. Benning, B. R. Horrocks, and D. A. Fulton, *Nanoscale*, 2013, **5**, 3817.

27 A. Benami, A. Lopez-Suarez, L. Rodriguez-Fernandez, A. Crespo-Sosa, J. C. Cheang-Wong, J. A. Reyes-Esqueda, and A. Oliver, *AIP Adv.*, 2012, **2**, 012193.

28 N. Gandra, C. Portz, L. M. Tian, R. Tang, B. G. Xu, S. Achilefu, and S. Singamaneni, *Angew. Chem. Int. Ed.*, 2014, **53**, 866.

29 M. Toma, U. Jonas, A. Mateescu, W. Knoll, and J. Dostalek, *J. Phys. Chem. C*, 2013, **117**, 11705.

30 C. Y. Zhang, H. C. Yeh, M. T. Kuroki, and T. H. Wang, *Nat. Mater.*, 2005, **4**, 826.

31 J. Cao, T. Sun, and K. T. V. Grattan, *Sens. Actuators B*, 2014, 195, 332.

32 X. Wu, X. X. He, K. M. Wang, C. Xie, B. Zhou, and Z. H. Qing, *Nanoscale*, 2010, **2**, 2244.

33 E. C. Cho, Y. Zhang, X. Cai, C. M. Moran, L. H. V. Wang, and Y. N. Xia, *Angew. Chem.Int. Ed.*, 2013, **52**, 1152.

34 F. R. Fan, D. Y. Liu, F. Y. Wu, S. Duan, Z. X. Xie, Z. Y. Jiang, and Z. Q. Tian, *J. Am. Chem. Soc.*, 2008, **130**, 6949.

35 J. X. Fang, S. Y. Du, S. Lebedkin, Z. Y. Li, R. Kruk, M. Kappes, and H. Hahn, *Nano Lett.*, 2010, **10**, 5006.

36 X. H. Liu, R. Huang, and J. Zhu, *Chem. Mater.*, 2008, **20**, 192.

37 L. H. Qian, B. Das, Y. Li, and Z. L. Yang, *J. Mater. Chem.*, 2010, **20**, 6891.

38 A. F. van Driel, I. S. Nikolaev, P. Vergeer, P. Lodahl, D. Vanmaekelbergh, and W. L. Vos, *Phys. Rev. B,* 2007, **75**, 035329.

39 T. J. Lin, W. J. Chuang, S. Cheng, Y. F. Chen, *Appl. Phys. Lett.*, 2009, **94**, 173506..